Water-mediated photo-induced reduction of platinum films

Authors

Jordi Fraxedas[a]*, Kuan Zhang[a], Borja Sepúlveda[a], María José Esplandiu[a], Xènia García de Andrés[b], Jordi Llorca[b], Virginia Pérez-Dieste[c] and Carlos Escudero[c]

[a] Catalan Institute of Nanoscience and Nanotechnology (ICN2), CSIC and BIST, Campus UAB, Bellaterra, Barcelona, 08193, Spain

[b] Institute of Energy Technologies, Department of Chemical Engineering and Barcelona Research Center in Multiscale Science and Engineering, Universitat Politècnica de Catalunya, EEBE, Eduard Maristany 10-14, Barcelona, 08019, Spain

[c] Alba Synchrotron Light Source, Carrer de la Llum 2-26, Cerdanyola del Vallès, Barcelona, 08290, Spain

Correspondence email: jordi.fraxedas@icn2.cat

Synopsis The beam damage produced by monochromatic soft X-ray photon beams on oxidized surfaces of platinum thin films is accelerated when water is condensed on such surfaces.

Abstract Platinum thin films activated ex situ by oxygen plasma become reduced by the combined effect of an intense soft X-ray photon beam and condensed water. The evolution of the electronic structure of the surface has been characterized by near-ambient pressure photoemission and mimics the inverse two-step sequence observed in electro-oxidation of platinum, *i.e.* the surface oxidized platinum species become reduced first and then the adsorbed species desorb in a second stage leading to a surface dominated by metallic platinum. The comparison with measurements performed under high vacuum conditions suggests that the reduction process is mainly produced by the reactive species generated by the radiolysis of water. When the photon flux is decreased, then the reduction process becomes slower.

Keywords: Beam damage, water, near-ambient pressure photoemission, platinum oxides.

1. Introduction

One of the intrinsic problems associated to synchrotron radiation delivered by high brilliance photon sources is the irreversible damage induced in the samples and in the optics by the intense beams (Storp, 1985; Henderson, 1995; Cazaux, 1997; Weik *et al*., 2000; Polvino *et al*., 2008; Meents et al. 2010; Nygård *et al.*, 2010; Garman & Weik, 2015; Spence 2017). The mechanisms behind beam damage are not completely understood and conform a complex example of the interaction of electromagnetic radiation with matter involving absorption, desorption, electronic excitations, thermal load, chemical and structural modifications, formation of defects, etc. The permanent quest for higher brilliance source makes this problem more acute in particular for soft materials (organic molecules, biomolecules and living cells), but also for supposedly robust inorganic materials. When the signal detection is fast enough the problem can be partially overcome by short exposure of the samples to the beam. This strategy is currently adopted *e.g.*, in the crystallography of biomolecules using ultra intense X-ray femtosecond pulses generated by free-electron lasers (Neutze *et al*., 2000; Emma *et al*., 2010). An alternative consists in reducing the photon flux by intentionally defocusing the X-ray beam or detuning the undulator in undulator-based beamlines, or using bending magnet beamlines, but a compromise has to be achieved in terms of energy or spatial resolution.

Synchrotron radiation experiments are performed in different environments, *i.e.* vacuum, controlled atmosphere (reactive or inert gases in a wide range of pressures, humidity), air, liquid, etc. and such environments may have an influence on the modification of the samples properties when combined with the photon beam. In the case of water, radiolysis is induced by the beam resulting in the formation of solvated electrons, e_{ap}^-, H•, HO• and HO_2• radicals, H_3O^+ and OH^- ions and molecular H_2 and H_2O_2 (Spinks & Woods, 1990). e_{ap}^- and H• are strongly reducing agents while HO• radicals are strongly oxidizing. Water radiolysis is affected at water/oxide interfaces since the electronic excitation mechanisms associated to the solid also play a role as, for example, in the generation of excitons (Le Caër, 2011). In addition, the water molecules can dissociate at the surface without the effect of the beam, which adds more complexity to the problem (Henderson, 2002).

Here, we study the combined effect of water and the photon beam leading to the irreversible modification of the surface of oxidized platinum films using Near-Ambient Pressure X-ray Photoemission Spectroscopy (NAP-XPS), a technique also termed Ambient Pressure X-ray Photoemission Spectroscopy (AP-XPS), that has enabled in the last years the study of the electronic structure of vapour/liquid/solid interfaces that are important for catalysis, atmospheric chemistry, and the interaction of water with solid surfaces at realistic operating pressures (Siegbahn, 1974; Salmeron & Schlögl, 2008; Trotochaud *et al*., 2017). Platinum is a relevant catalyst (Ertl, 2008) and the oxidation of its surfaces has been extensively studied using different experimental techniques such as photoemission (Kim *et al*., 1971), X-ray absorption (Miller *et al*., 2011; Miller *et al.*, 2014), NAP-XPS (Arrigo *et al*., 2013; Axnanda *et al*., 2015; Saveleva *et al.*, 2016; Takagi *et al.*, 2017), scanning

tunnelling microscopy (Zhu *et al*., 2012; van Spronsen et al., 2017), electrochemical (Conway, 1995; Gomez-Marin *et al*., 2013) or surface-enhanced Raman spectroscopy (Luo *et al*., 2000) to mention a few techniques. In particular, we are interested in platinum/silicon systems because they are the base of photochemically propelled micro/nanomotors whose motion can be externally activated by light using water or H_2O_2 as a fuel (Esplandiu *et al*. 2018). In such systems two competing mechanisms are involved in the propulsion, namely self-electro- and diffusio-phoresis/osmosis, respectively (Zhang *et al*., 2017). The former involves the generation of electron-hole pairs in the silicon, which act as reducing and oxidizing agents at the platinum and silicon surfaces, respectively, while the later involves oxidation and reduction reactions only at the metal side.

2. Experimental details

We have used 10 mm x 10 mm p-type silicon substrates with one half covered with a 50 nm thick Pt film grown ex-situ by e-beam deposition (see Figure S1). All samples were ex-situ activated with oxygen plasma (1 min. at 360 Watts) and then stored under nitrogen atmosphere prior to the experiments. The samples were measured after 1-2 days of the plasma treatment without any ulterior preparation.

The resulting silicon oxide layer exhibits a thickness of about 2.3 nm, as determined from the peak areas ratio of both Si2p lines (the measured thickness of the native oxide layer in silicon is 0.8 nm) (Himpsel *et al*., 1988). The platinum part has been used as a reference for energy calibration. Binding energies are referred to the $Pt4f_{7/2}$ peak of metallic platinum (71.0 eV), as determined for analogous ex-situ grown unactivated films (no exposure to oxygen plasma) with the silicon part covered with a gold film ($Au4f_{7/2}$ peak located at 84.0 eV, which confirms correct energy calibration) and using a PHOIBOS150 hemispherical analyser from SPECS with a monochromatic X-ray source (1486.6 eV) located at ICN2. A least-square fit using the CasaXPS software (Walton et al., 2010) to the Pt4f lines after subtraction of a Shirley-type background provides a branching ratio $Pt4f_{5/2}/Pt4f_{7/2}$=3/4 and a spin orbit splitting of 3.3 eV using an asymmetric (Gelius-type) line shape.

NAP-XPS experiments were performed at the NAPP endstation of the BL-24 CIRCE undulator beamline, in the ALBA synchrotron light source (Pérez-Dieste *et al.* 2013). The NAPP endstation is equipped with a PHOIBOS NAP150 XPS analyser (SPECS) and a differential pumping system for operating at pressures up to approximately 10 mbar. The beam spot size at the sample was around 100 (horizontal) μm × 20 (vertical) μm. Ultrapure water ("Ultrapur" from MERCK) was degassed by repeated cycles of liquid nitrogen freeze-pump-thaw before introduction into the analysis chamber from a glass vessel via a precision leak valve. Water condensation was achieved by cooling the sample with a Peltier device. The used photon energies were 220 and 680 eV in order to achieve high surface sensitivity for both platinum (Pt4f) and oxygen (O1s) components, respectively, and the emitted photoelectrons were acquired with a pass energy of 10 eV.

3. Experimental results

3.1. High vacuum and room temperature

Figure 1(a) shows a XPS spectrum of the Pt4f line (continuous black line) of an as-received sample and a least-square fit after a Shirley-type background subtraction (continuous orange line) using 4 spin-orbit components. The spectrum was obtained with 680 eV photons in a 10^{-6} mbar base pressure and at room temperature. The blue components correspond to a Gelius-type asymmetric line shape in order to account for hole screening effects while the rest (red, olive and green) are symmetric. The following constraints were used: (i) same branching ratio and spin-orbit splitting for all components and (ii) identical FWHM only for the symmetric components. The features with 71.0, 72.1, 72.9 and 74.1 eV binding energies correspond to metallic platinum (blue), platinum with oxygen/hydroxide adsorbed on the surface (red, Pt-O_{ads}/OH) (Zhu *et al*., 2012), PtO (olive, Pt^{2+}) and PtO_2 (green, Pt^{4+}), respectively (Kim *et al.*, 1971; Arrigo *et al.*, 2013; Saveleva *et al.*, 2016). The envelope from the fit is represented by the discontinuous grey line, which closely follows the (non-smoothed) experimental data. The FWHM for the 71.0 eV feature is 0.57 eV and 1.4 eV for the rest of components.

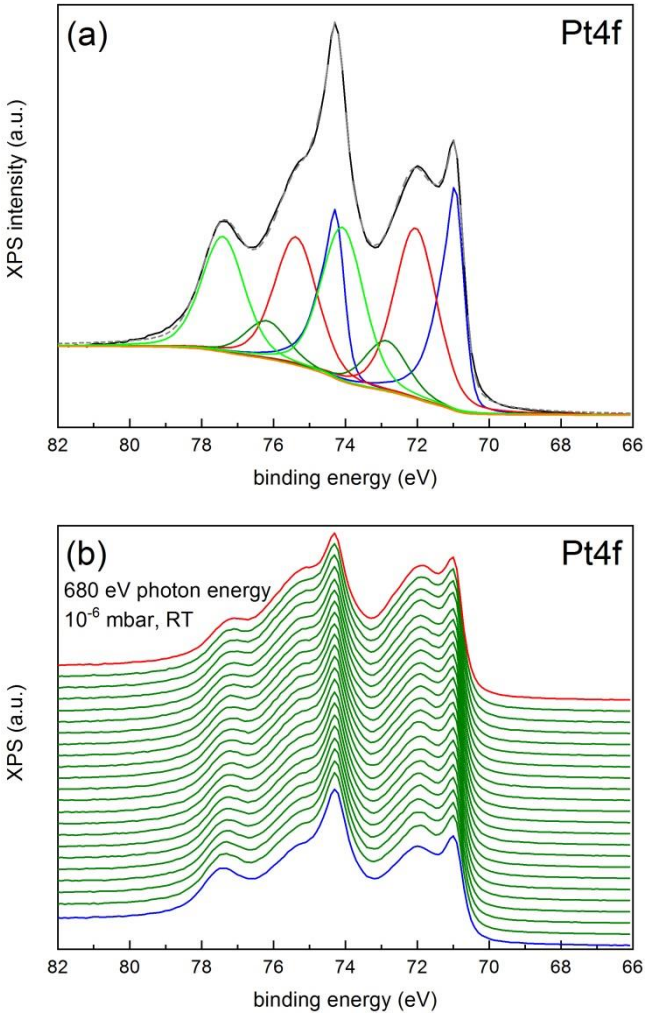

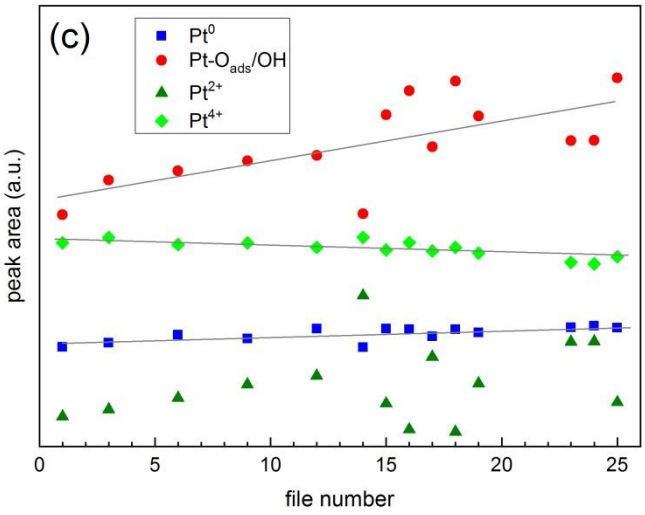

Figure 1 Photoemission spectra of the Pt4f line taken with 680 eV photons at 10^{-6} mbar and room temperature on the Pt film: (a) least-square fit after a Shirley-type background subtraction using 4 components (see main text for details) and (b) evolution of the spectra after 44 minutes exposure of the beam at the same spot. The spectra have been shifted with a fixed offset along the intensity axis for clarity. (c) Evolution of the areas of the $Pt4f_{7/2}$ peaks as a function of the sequentially acquired spectra: full blue square, red circle, olive triangle and green diamond represent metallic Pt, Pt-O_{ads}/OH, PtO and PtO_2, respectively. The grey lines are guides to the eye.

Figure 1(b) shows the evolution of the photoemission spectra of the Pt4f lines acquired continuously at the same sample spot during 44 minutes at 10^{-6} mbar with an estimated photon flux of 2.6×10^{11} ph/s. The first and last spectra correspond to the continuous blue and red lines, respectively. Prior to the acquisition of the first spectrum, the distance between the sample surface and the entrance of the analyser cone (see Figure S1) was optimized in a given surface location and then the sample was moved to a fresh region by moving the sample horizontally at a distance above the lateral dimension of the beam spot (100 μm). From the figure we observe the decrease in intensity of the $Pt4f_{5/2}$ feature at 77.4 eV binding energy, associated to PtO_2. Figure 1(c) shows the evolution of the areas of the $Pt4f_{7/2}$ peaks as a function of the sequentially acquired spectra. From the figure we observe a steady increase of both the Pt-O_{ads}/OH and metallic Pt features, with a dominant effect for the Pt-O_{ads}/OH signal, and a slight decrease of the Pt^{4+} signal. The evolution of the Pt^{2+} feature is less reliable because of the proximity of the dominant Pt-O_{ads}/OH peak and the asymmetric tail of the metallic Pt contribution, which induces a certain degree of uncertainty in the fit.

3.2. Near ambient pressure and low temperature

After the experiments described above, the analyser chamber was filled with 3 mbar water vapour and the sample stage was cooled down to 0 degrees C. Figure 2(a) shows the evolution of the

photoemission spectra of the Pt4f lines acquired continuously at the same sample spot during 19 min with an estimated photon flux of about 2.5×10^{11} ph/s. Again, the first (fresh sample region) and last spectra correspond to the continuous blue and red lines, respectively. Figure 2(b) shows the evolution of the areas of the $Pt4f_{7/2}$ peaks as a function of the sequentially acquired spectra. From the figure we observe a reduction of the platinum species with a steady increase of the metallic Pt feature (full blue square) and a decrease of the components corresponding to different oxidation states, with a plateau for the Pt-O_{ads}/OH signal at the early stages of irradiation.

An analogous experiment was performed in a fresh sample region but for 33 min. After acquisition of the last spectrum the sample was no longer exposed to the photon beam (beam shutter closed) and kept under 3 mbar water vapour pressure and at 0 degrees C for 25 minutes. Then a spectrum was obtained at the same previous measured sample region. The results are shown in Fig. S2, where the last spectrum of the first series and the new one are represented by continuous blue and red lines, respectively. No changes between both spectra can be observed. Thus, the exposure of the reduced (metallic) surface to condensed water does not lead to oxidation.

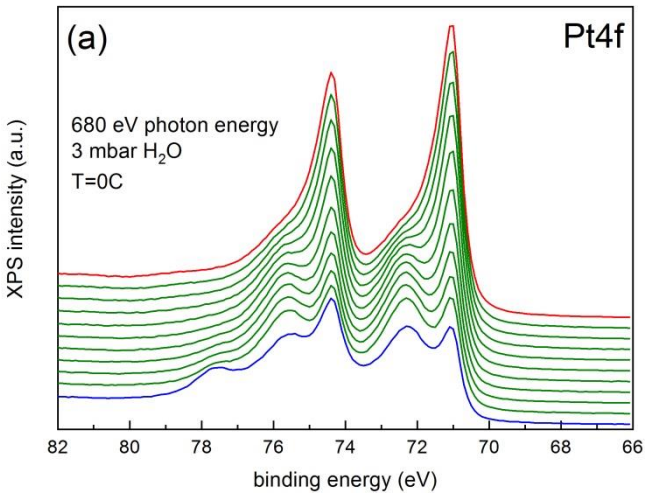

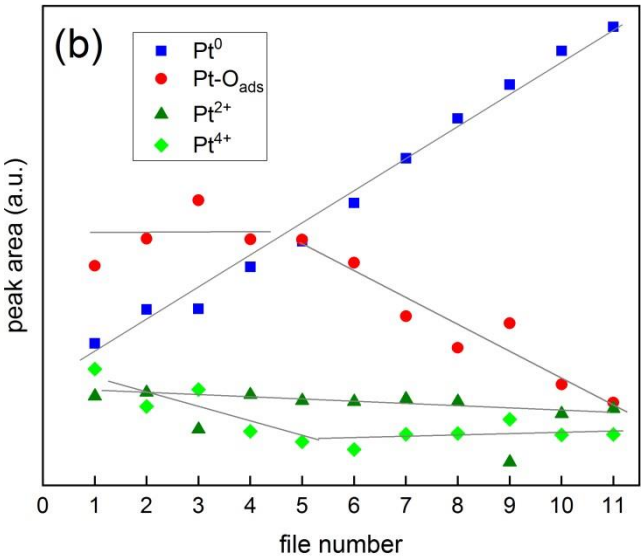

Figure 2 (a) Photoemission spectra of the Pt4f line taken with 680 eV photons at 3 mbar of water vapour and at 0 degrees C. The spectra have been shifted with a fixed offset along the intensity axis for clarity. (b) Evolution of the areas of the $Pt4f_{7/2}$ peaks as a function of the sequentially acquired spectra: full blue square, red circle, olive triangle and green diamond represent metallic Pt, Pt-O_{ads}/OH, PtO and PtO_2, respectively. The grey lines are guides to the eye.

The redox reduction of the platinum film here reported is clearly accelerated by the presence of water, as results from the comparison between Figs. 1(b) and 2(a). Water condenses on the platinum surface as depicted from Fig. 3. In this figure the XPS O1s line is compared when the sample is under high vacuum and room temperature (continuous blue line) with the case when the sample is exposed to 3 mbar and at 0 degrees conditions (continuous red line). The blue curve shows two main components with a shoulder at about 530.4 eV and a main feature centred at 531.4 eV binding energies, mainly arising from Pt-O and Pt-OH species, respectively (Arrigo *et al*., 2013). The red curve shows a prominent peak at 535.1 eV arising from the water gas phase and a peak centred at 532.7 eV. This peak arises from molecularly adsorbed (intact) water (Ketteler *et al*., 2007; Miller *et al*., 2011; Lampimäki *et al*., 2015; Macías-Montero *et al*., 2017). Note that at 10^{-6} mbar, the formation of a monolayer of water per second is expected, so that the asymmetry of the main feature towards higher binding energies may arise from the presence of condensed water at the surface, which is emphasized due to the high surface sensitivity of 150eV kinetic energy electrons.

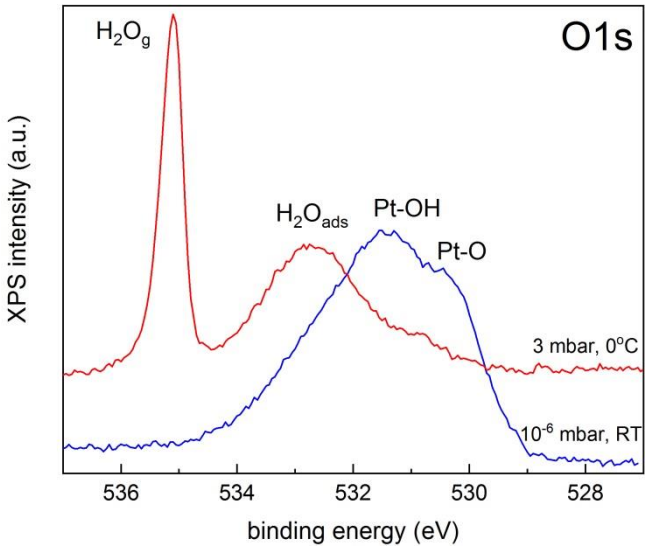

Figure 3 XPS O1s lines measured at the Pt film at high vacuum and room temperature (continuous blue line) and at 3 mbar water vapour and 0 degrees C (continuous red line) with 680 eV photons.

Figure 4(a) shows the evolution of the photoemission spectra of the Pt4f lines acquired continuously at the same sample spot during 31 min with 220 eV photons at 3 mbar water vapour and 0 degrees C, with an estimated photon flux of 2.2×10^{11} ph/s. Again, the first and last spectra correspond to the continuous blue and red lines, respectively. Figure 4(b) shows the evolution of the areas of the $Pt4f_{7/2}$ peaks as a function of the sequentially acquired spectra. From the figure we observe a steady increase of the metallic Pt features and a decrease of both Pt^{2+} and Pt^{4+} signals and a nearly constant Pt-O_{ads}/OH signal.

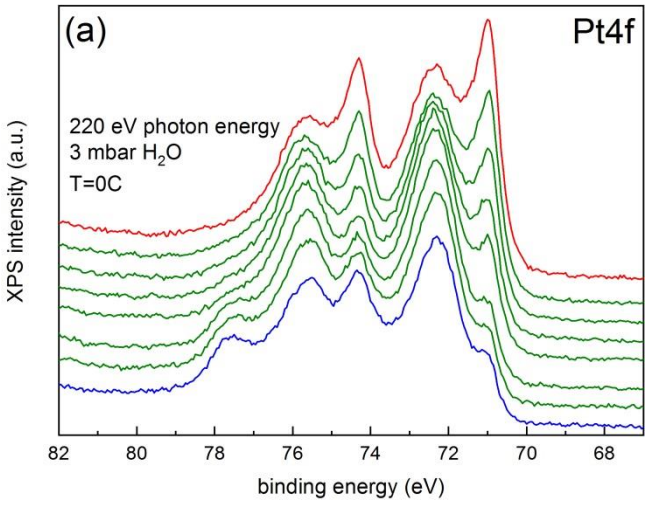

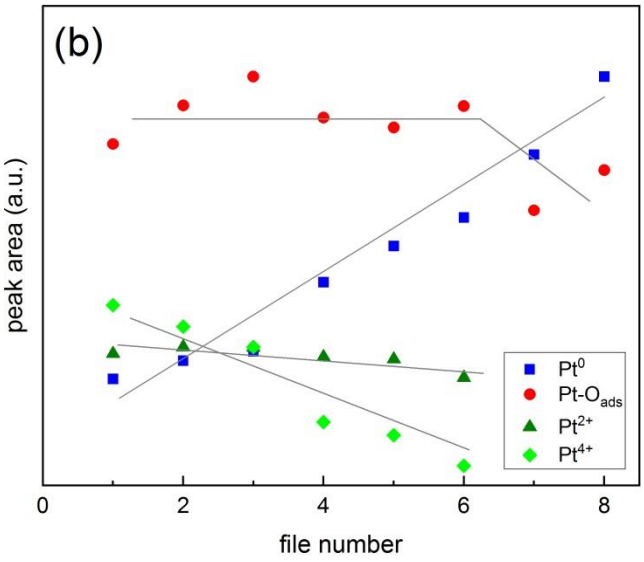

Figure 4 (a) Photoemission spectra of the Pt4f line taken with 220 eV photons at 3 mbar of water vapour and at 0 degrees C. The spectra have been shifted with a fixed offset along the intensity axis for clarity. (b) Evolution of the areas of the $Pt4f_{7/2}$ peaks as a function of the sequentially acquired spectra: full blue square, red circle, olive triangle and green diamonds represent metallic Pt, Pt-O_{ads}/OH, PtO and PtO_2, respectively. The grey lines are guides to the eye.

4. Discussion

Figures 1, 2 and 4 evidence that the redox reduction of the platinum films is accelerated by the presence of condensed water while exposed to the intense beam. From the experiments we observe that the PtO and PtO_2 reduction occurs first and that the desorption of Pt-O_{ads}/OH occurs in a second stage. This evolution corresponds to the inverse sequence observed in electro-oxidation of platinum, where during the first stages O/OH adsorbates are formed with the subsequent nucleation and 3D growth of oxides (Saveleva et al., 2016). The observed evolution in the present work becomes more evident when the beam flux is decreased, as shown in Fig. 5. The data were acquired maintaining the same experimental conditions as in Fig. 2(a), that is with 680 eV photons, under a water vapour pressure of 3 mbar and with the sample at 0 degrees C, but measuring at the same sample spot during 49 min with a 6-fold lower photon flux as compared to the spectra in Fig. 2(a). The 3 D plot evidences that while the intensity corresponding to the Pt^{4+} features decreases, the intensity of the peak corresponding to O_{ads}/OH increases and the feature assigned to metallic platinum remains essentially constant in a first stage. At some point, at about two thirds of the sequence, the intensity of the O_{ads}/OH peak decreases and the feature corresponding to metallic platinum increases. Thus, in the first stage, part of the oxygen atoms of the oxide species is transferred to the surface and becomes adsorbed. The fact that the reduction process becomes slower with lower beam flux is a proof that the

reduction is mainly due to the beam intensity and related events, as secondary electrons emission, and to a lesser or none extent to dissociated water molecules arising from the water/surface interaction.

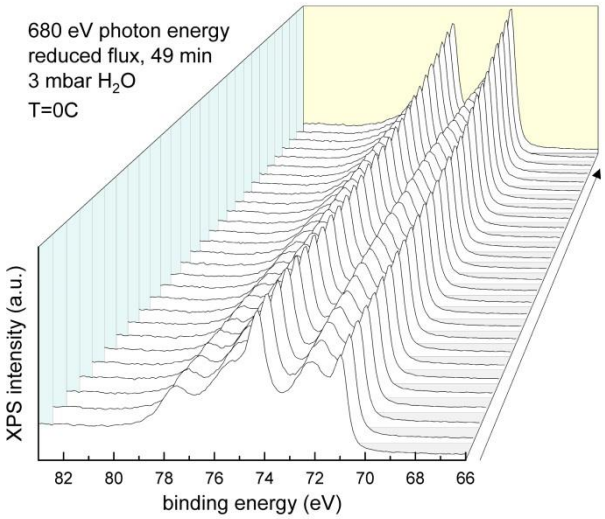

Figure 5 3D plot of the evolution of the photoemission spectra of the Pt4f line taken with 680 eV photons at 3 mbar of water vapour and at 0 degrees C under a photon beam flux that has been decreased by a factor of 6 as compared to the data shown in Fig. 2(a). The time lapse from the first (front) to the last spectra is 49 min. The arrow indicates the temporal evolution. All spectra have been acquired at the same sample position.

We associate the accelerating role of water to the radiolysis of condensed water caused by the beam. As mentioned above, the beam generates radicals, ions and molecular species that can interact with the surface. Moreover, one has to take into account the electronic excitations at the oxide surfaces that can lead to chemical reactions in addition to the generation of secondary electrons. Thus, although we do not have experimental evidence of the presence of reactive water fragments, we hypothesize that the reduction observed at the platinum surfaces is mainly originated by the presence of highly reactive species. Such species may contribute to the broadening of the O1s line, since the time scale of the generation of such species and the photoemission process are of the same order of magnitude (about 10^{-13} s.). One may tentatively associate the observed reduction to the strongly reducing agents e_{aq}^- and H•, although other species may play a role. As mentioned earlier the reduction observed at 10^{-6} mbar is much smaller but not negligible and this may be explained by the formation of a monolayer of water per second at such pressure (Redhead et al., 1993).

Beam damage is less significant on the silicon oxide surface (see Fig. S1). Figure S3 depicts the evolution of the Si2p peaks which points towards a slight charging effect, as evidenced by the shift of the oxide peak (104.1eV) towards higher binding energies, as well as an increase of the background

(Lazzarino et al., 2002; Verdaguer *et al*., 2007; Evangelio *et al*., 2017). The increase of the background can be ascribed to the generation of defects due to the beam and is independent of the presence of condensed water (Le Caër, S., 2011; Evangelio *et al*. 2017).

5. Conclusions

We have shown by means of near-ambient pressure photoemission experiments that ex situ activated platinum films (prepared under oxygen plasma conditions) become reduced by the combined effect of an intense soft X-ray photon beam and condensed water. The reduction processes closely follows the inverse mechanisms found in electro-oxidation of platinum. Here we observe, in a first stage, the reduction of the Pt^{4+} and Pt^{2+} species with a parallel increase of the signals assigned to adsorbed oxygen and metallic platinum. In a second stage adsorbed oxygen desorbs increasing the metallic character of the surface. The reduction rate is lowered both when the condensed water amount and the photon flux are decreased and the exposure to condensed water of the metallic surface does not lead to oxidation. With such experimental evidences we hypothesise that the observed reduction is mainly induced by the reactive species generated through the radiolysis of water, although we do not have a direct experimental proof of their existence.

Acknowledgements The authors would like to thank the support of ALBA staff for the successful performance of the measurements at the NAPP branch of the CIRCE beamline from the ALBA Synchrotron Light Source. We thank Dr. G. Sauthier for helping in the XPS measurements performed with the ICN2 XPS system. JL is Serra Húnter Fellow and is grateful to ICREA Academia program.

References

Arrigo, R., Hävecker, M., Schuster, M. E., Ranjan, C., Stotz, E., Knop-Gericke, A. & Schlögl, R. (2013). Angew. Chem. Int. Ed. 52, 11660-11664.

Axnanda, S., Crumlin, E. J., Mao, B., Rani, S., Chang, R., Karlsson, P. G., Edwards, M. O. M., Lundqvist, M., Moberg, R., Ross, P., Hussain, Z. & Liu, Z. (2015) Sci. Rep. 5, 9788.

Chan, H. Y. H., Zou, S. & Weaver, M. J. (1999) J. Phys. Chem. B 103, 11141-11151.

Cazaux, J. (1997) J. Microsc. 188, 106–124.

Conway, B.E. (1995) Prog. Surf. Science 49, 331-452.

Emma, P., Akre, R., Arthur, J., Bionta, R., Bostedt, C., Bozek, J., Brachmann, A., Bucksbaum, P., Coffee, R., Decker, F.-J., Ding, Y., Dowell, D., Edstrom, S., Fisher, A., Frisch, J., Gilevich, S., Hastings, J., Hays, G., Hering, Ph., Huang, Z., Iverson, R., Loos, H., Messerschmidt, M., Miahnahri,

A., Moeller, S., Nuhn, H.-D., Pile, G., Ratner, D., Rzepiela, J., Schultz, D., Smith, T., Stefan, P., Tompkins, H., Turner, J., Welch, J., White, W., Wu, J., Yocky, G. & Galayda, J. (2010) Nature Photonics 4, 641–647.

Ertl, G. (2008) Angew. Chem. Int. Ed. 47, 3524–3535

Esplandiu, M. J., Farniya, A. A. & Bachtold, A. (2015) ACS Nano 9, 11234-11240.

Esplandiu, M. J., Zhang, K., Fraxedas, J., Sepúlveda, B. & Reguera D. (2018). Acc. Chem. Res., 51, 1921–1930.

Evangelio, L., Gramazio, F., Lorenzoni, M., Gorgoi, M., Espinosa, F.M., García, R., Pérez-Murano, F. & Fraxedas, J. (2017). Beilstein J. Nanotechnol. 8, 1972–1981.

Garman, E. F. & Weik, M. (2015) J. Synchrotron Rad. 22, 195-200.

Gomez-Marin, A.M., Clavilier, J., & Feliu, J.M. (2013) J. Electroanal. Chem. 688, 360-370.

Henderson, R. (1995) Q. Rev. Biophys. 28, 171–193.

Henderson, M. A. (2002). Surf. Sci. Rep. 46, 1-308.

Himpsel, F. J., McFeely, F. R., Taleb-Ibrahimi, A., Yarmoff, J. A. & Hollinger, G. (1988) Phys. Rev. B 38, 6084-6096.

Ketteler, G., Yamamoto, S., Bluhm, H., Andersson, K., Starr, D. E., Ogletree, D. F., Ogasawara, H., Nilsson, A. & Salmeron, M. (2007) J. Phys. Chem. C 111, 8278–8282.

Kim, K. S., Winograd, N. & Davis, R. E. (1971). J. Am. Chem. Soc. 93, 6296-6297.

Lampimäki, M., Schreiber, S., Zelenay, V., Křepelová, A., Birrer, M., Axnanda, S., Mao, B., Liu, Z., Bluhm, H. & Ammann, M. (2015) J. Phys. Chem. C 119, 7076.

Lazzarino, M., Heun, S., Ressel, B., Prince, K. C., Pingue, P. & Ascoli, C. (2002) Appl. Phys. Lett., 81, 2842.

Le Caër, S. (2011) Water 3, 235-253.

Luo, H., Park, S., Chan, H. Y. H. & Weaver, M. J. (2000) J. Phys. Chem. B 104, 8250-8258.

Macías-Montero, M., López-Santos, C., Filippin, A. N., Rico,V. J., Espinós, J. P., Fraxedas, J., Pérez-Dieste, V., Escudero, C., González-Elipe, A. R. & Borrás, A. (2017) Langmuir 33, 6449−6456.

Meents, A., Gutmann, S., Wagner, A. & Schulze-Briese, C. (2010) Proc. Natl. Acad. Sci. USA 107, 1094–1099.

Miller, D. J., Öberg, H., Kaya, S., Sanchez Casalongue, H., Friedel, D., Anniyev, T., Ogasawara, H., Bluhm, H., Petterson, L. G. M. & Nilsson, A. (2011). Phys. Rev. Lett. 107, 195502.

Miller, D., Sanchez Casalongue, H., Bluhm, H., Ogasawara, H., Nilssom, A. & Kaya, S. (2014) J. Am. Chem. Soc. 136, 6340-6347.

Neutze, R., Wout, R., van der Spoel, D., Weckert, E. & Hajdu, J. (2000) Nature 406, 752–757

Nygård, K., Gorelick, S., Vila-Comamala, J., Färm, E., Bergamaschi, A., Cervellino, A., Gozzo, F., Patterson, B. D., Ritala, M. & David, C. (2010) J. Synchrotron Rad. 17, 786-790

Pérez-Dieste, V., Aballe, L., Ferrer, S., Nicolas, J., Escudero, C., Milán & Pellegrin, E. (2013). J. Phys. Conf. Ser. 425, 072023.

Polvino, S. M., Murray, C. E., Kalenci, Ö., Noyan I. C., Lai, B. & and Cai, Z. Appl. Phys. Lett. (2008) 92, 224105.

Redhead, P.A., Hobson, J. P. & Kornelsen, E. V. (1993) The Physical Basis of Ultrahigh Vacuum, American Institute of Physics, New York.

Salmeron, M. & Schlögl, R. (2008) Surf. Sci. Rep. 63, 169-199.

Saveleva, V. A., Papaefthimiou, V., Daletou, M. K., Doh, W. H., Ulhaq-Bouillet, C., Diebold, M., Zafeiratos, S. & Savinova, E. R. (2016). J. Phys. Chem. C 120, 15930-15940.

Siegbahn, K. (1974) J. Electron Spectrosc. Rel. Phenom. 5, 3-97.

Spence, J. C. H. (2017) Struct Dyn. 4, 044027.

Spinks, J. W. T. & Woods, R. J. (1990) An Introduction to Radiation Chemistry, 3rd ed.; Wiley-Interscience publication: New York, NY, USA.

Storp, S. (1985) Spectrochimica Acta Part B: Atomic Spectroscopy 40, 745-756.

Trotochaud, L., Head, A. R., Karslıoğlu, O., Kyhl, L. & Bluhm, H. (2017) J. Phys.: Cond. Matt. 29, 053002.

Takagi, Y., Wang, H., Uemura, Y., Nakamura, T., Yu, L., Sekizawa, O., Uruga, T., Mizuki, (2017) Phys.Chem.Chem.Phys.19, 6013

van Spronsen, M. A., Frenken, J. W. M. & Groot, I. M. N. (2017) Nature Commun. 8, 429.

Verdaguer, A., Weis, Ch., Oncins, G., Ketteler, G., Bluhm, H. & Salmeron, M. (2007) Langmuir 23, 9699-9703.

Walton, J., Wincott, P., Fairley, N., & Carrick, A. (2010). Peak Fitting with CasaXPS: A Casa Pocket Book. Knutsford, UK: Accolyte Science.

Weik, M., Ravelli, R. B. G., Kryger, G., McSweeney, S, Raves, M. L., Harel, M., Gros, P., Silmani, I., Kroon, J. & Sussman, J. L. (2000) Proc. Natl. Acad. Sci. USA 97, 623–628.

Zhang, K., Fraxedas, J., Sepúlveda, B. & Esplandiu, M. J. (2017). ACS Appl. Mater. Interfaces, 9, 44948–44953.

Zhu, Z., Tao, F., Zheng, F., Chang, R., Li, Y., Heinke, L., Liu, Z., Salmeron, M. & Somorjai, G, A. (2012) Nano Lett. 12, 1491-1497.